76015

Vesicular Micropoikilitic Impact Melt Breccia 2819 g, 20 x 16 x 14cm

INTRODUCTION

Sample 76015 was chipped off of the top corner of Block 5 of the big boulder at Station 6 (Fig. 1, Wolfe and others, 1981). It is a sample of lithologic unit B of Boulder 6 and is similar in color and texture to 76215 from Block 4 (also from unit B). This lithology was originally referred to as the "green-grey" breccia lithology (Fig. 2). 76015 has a well-documented orientation based on laboratory photography and has a well-known exposure history because of its certain relationship to several other samples of the Station 6 Boulder (Heiken et al., 1973).

One surface of 76015 was part of a shielded cavity that was oriented parallel to the sunline, which had an azimuth of approximately 106 deg and elevation of approximately 36 deg to the horizontal. This unique cavity has allowed several interesting studies of the solar flare, cosmic ray, and micrometeorite bombardment of the lunar surface (Blanford et al.,1974; Morrison and Zinner, 1975; Crozaz et al.,1974). The "lip" of this cavity has a thick, undisturbed patina (Fig. 3).

Spudis and Ryder (1981) summarize the arguments that this boulder is from the melt sheet or ejecta blanket from the Serenitatus impact event. Simonds et al. (1976) and Onorato et al. (1976) provide a comprehensive thermal model for the lithification of impact melt breccias based on their detailed study of the textures of samples from Boulder 6 and in comparison with melt sheets from large terrestrial craters.

PETROGRAPHY

Sample 76015 is a very vesicular, crystalline-matrix breccia with X0.1 mm to 5 cm long irregular vesicles that compose about 20% of the rock by volume. The flattened

Figure 1: Location of 76015 on Block 5 before sampling. Note the well-documented orientation. AS17-140-21411.

Figure 2: The exterior surface of 76015 has been heavily eroded by micrometeorite bombardment and is covered with glass-lined micrometeorite craters (zap pits) with white spall zones. The foliation of the abundant large vesicles is evident in this photo. Scale is 1 cm. S73-15015.

vesicles define a preferred orientation best seen on the west (W1) side of the sample (Fig. 2). The modal mineralogy of 76015 is about 50% plagioclase, 40% low-calcium pyroxene, with minor amounts of augite, olivine, ilmenite, armalcolite, and metallic iron. The poikilitic matrix of 76015 (Fig. 4) consists of a nearly continuous mass of elongated and occasionally aligned 0.2-0.3 by 0.7-1.5 mm low-calcium pyroxene oikocrysts ($Wo_{4-9}En_{61-76}Fs_{19-25}$)• Tabular feldspar 10-50 µm long occurs both within and between the pyroxene grains and ranges from An_{82} to An_{96}, with a distinct peak at An_{89} (Fig. 5). Small amounts of augite ($W0_{35-40}En_{42-46}Fs_{l2-15}$) are found as <20 µm grains both within and between the low-calcium pyroxene oikocrysts. Both poikilitic ilmenite and armalcolite grains up to 200 µm long, with spinel and ruffle lamellae, are concentrated between the pyroxene oikocrysts.

Mineral and lithic clasts compose 5-15% of the rock. Mineral clasts are recognized because they are typically over 50 µm across, much larger than the matrix grains. Simonds et al. (1974 and 1975) studied numerous small lithic clasts in 22 thin sections of 76015 and found that they were predominantly granoblastic or poikilitic in texture, generally with 70-80% feldspar. Some of the small clasts were described as annealed "dunite" and "troctolite" fragments.

Simonds (1975) describes the poikilitic matrix of 76015 as a continuous network of interlocking pigeonite oikocrysts with about half of the pyroxene in a tight cluster in the compositional diagram $Wo_{5-6}En_{70-73}Fs_{22-26}$. Simonds notes that the narrow range of pyroxene and feldspar composition agrees with the uniform compositional data of Rhodes et al. (1974) and Hubbard et al. (1974) for widely separated portions of the sample. They conclude that the matrix of this sample is very homogeneous in composition.

Figure 3: This photo of 76015 illustrates the patina covered "lip" that was partially shielded from micrometeorites (see text). The large vesicular basalt "vug" class is evident in the center of the photo. Scale is 1 cm. S73-18764.

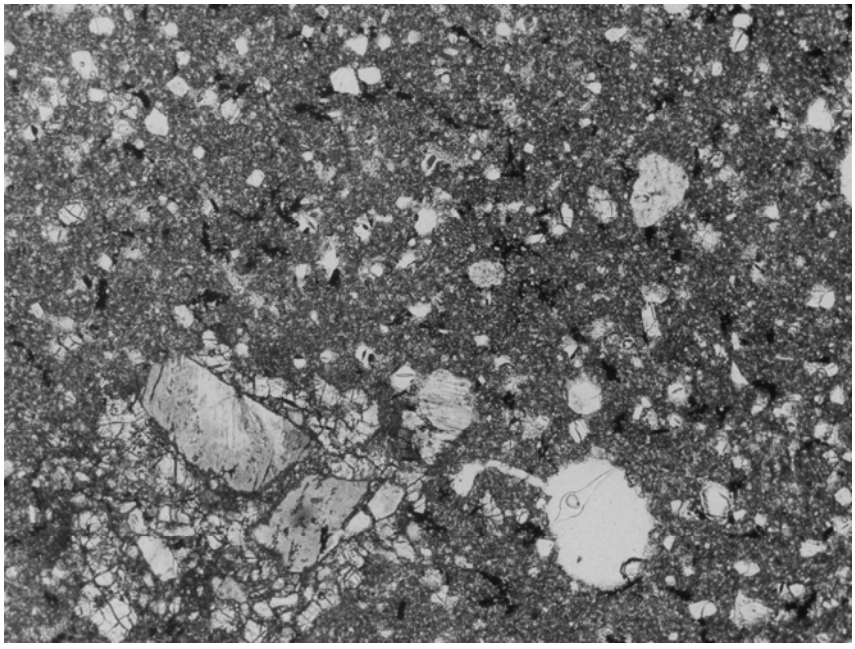

Figure 4: Photomicrograph of 76015 matrix. Note the partially digested relict clast and the large vesicle. The texture of the matrix of 76015 is poikilitic with large pyroxene grains surrounding small plagioclase laths and mineral inclusions. This texture is typical of the matrix of all the Station 6 boulders as well as many Apollo 16 melt rocks. Field of view is 4 x 5 mm.

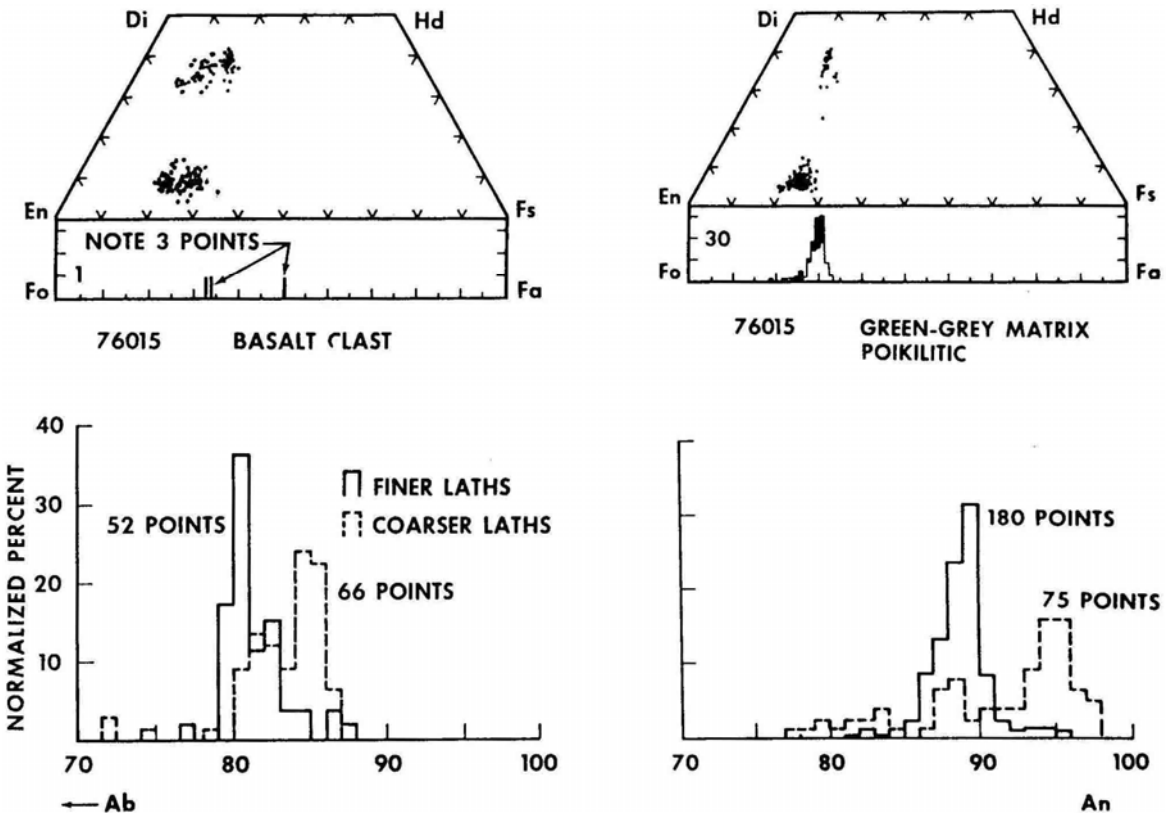

Figure 5: Pyroxene, olivine, and plagioclase compositions of the matrix and the vesicular basalt clast in lunar breccia 76015 (from Simonds, 1975). Note that the larger plagioclase inclusions in the green-grey matrix are more calcic (An_{95}) than the plagioclase laths in the matrix (An_{89}).

Misra et al. (1976) have studied the complex metallic nickel-iron particles included in 76015 (Fig. 6).

WHOLE-ROCK CHEMISTRY

The matrix of 76015 is very homogeneous in composition (Table 1) and the composition is also very similar to that of the other samples of this boulder (Fig. 7).

Higuchi and Morgan (1975) find that the trace siderophile element compositions of all the samples of the Station 6 Boulder form a tight grouping (meteorite group 2) on compositional diagrams (Fig. 8). 76015 and 76215 have a lower abundance of these meteoritic elements than the matrix for 76275 and 76295 (Table 2).

SIGNIFICANT CLASTS

Simonds (1975) and Phinney (1981) describe a large (2 cm) porous basalt clast ("vug" filling?) in 76015 with intersertal texture (Fig. 9). The plagioclase in this clast is found to be somewhat less calcic than that of the breccia matrix (Fig. 5). However, there appear to be no chemical or isotopic data on this large basalt clast (see also Fig. 3).

RADIOGENIC ISOTOPES

Cadogan and Turner (1976) determined the crystallization age of 76015 by the ^{39}Ar-^{4O}Ar plateau technique. The matrix yielded an intermediate temperature plateau which covered 70% of the release of ^{39}Ar and corresponds to an age of 3.93 ± 0.04 b.y. A similar but less well-defined age of 3.96 ± 0.06 b.y. was obtained for a plagioclase separate (Fig. 10).

Nyquist et al. (1974) have reported Rb-Sr data for several splits of matrix from 76015 (Fig. I 1 and Table 3) and note that the Rb-Sr

systematics are probably partially reset by the Serenitatus impact event (see Phinney, 1981). U-Th-Pb data by Leon Silver were also reported in Phinney (1981).

COSMOGENIC RADIOISOTOPES AND EXPOSURE AGES

Crozaz et at. (1974) have studied the long-term exposure history of a surface of 76015 that was exposed to the sky through a small solid angle (as evidenced by a marked gradient of dark to light patina) (see figure in their paper). As a consequence of the small solid angle factor, the effects of erosion over a long period of time are removed, allowing for a study of the solar flare spectrum without the complication of continuous erosion. Indeed, the measured solar flare track density for 76015 was found to fall off much faster with depth than for other lunar samples (which have experienced erosion) and is comparable with data on the energy of solar flares derived by studies of recent solar flares using the Surveyor glass (Crozaz et al.). The solar flare track exposure age (18 ± 3 m.y.) is found to be concordant with the galactic proton age (17.5 ± 0.5 m.y.) as determined by the Kr-Kr method, although somewhat younger than the 22 m.y. exposure age determined for 76315 (Arvidson et al., 1975). Presumably a portion of the surface of 76015 eroded away in the past (Crozaz et al.).

Bogard et al. (1974) (see unpublished data in Phinney, 1981) have determined the noble gas abundances in 76015.

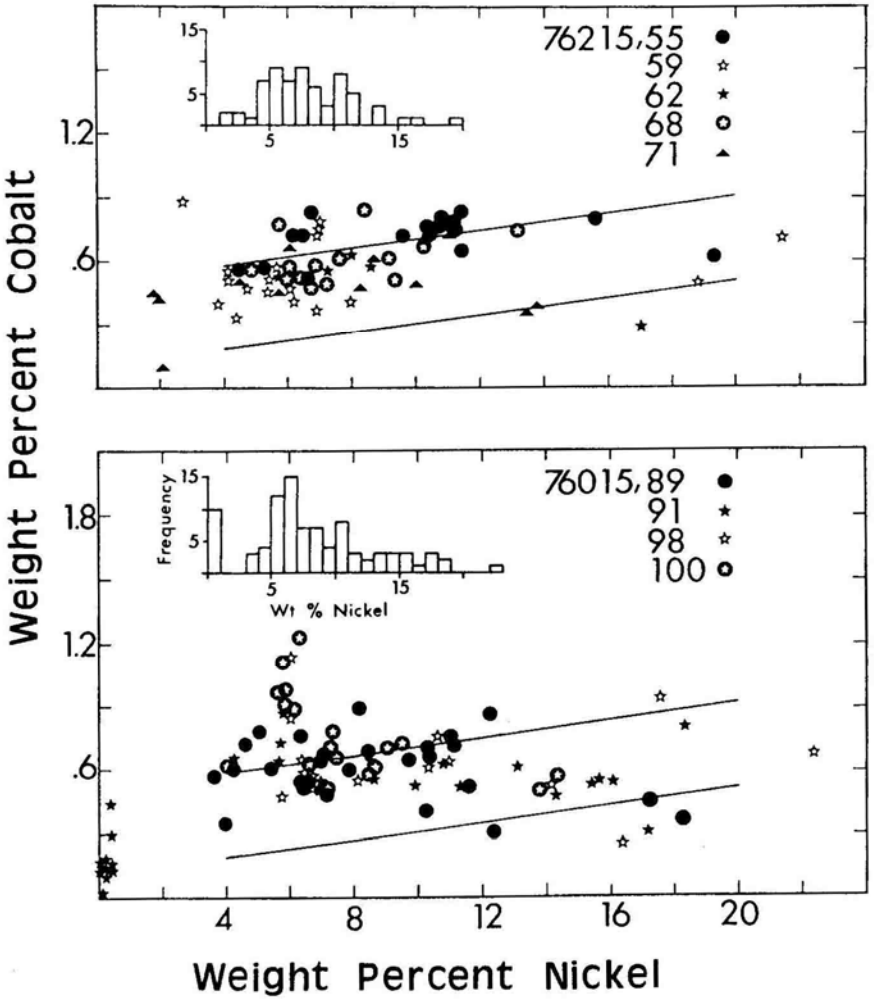

Figure 6: Nickel vs. cobalt contents of metal grains in 76015 and 76215. From Misra et al. (1976).

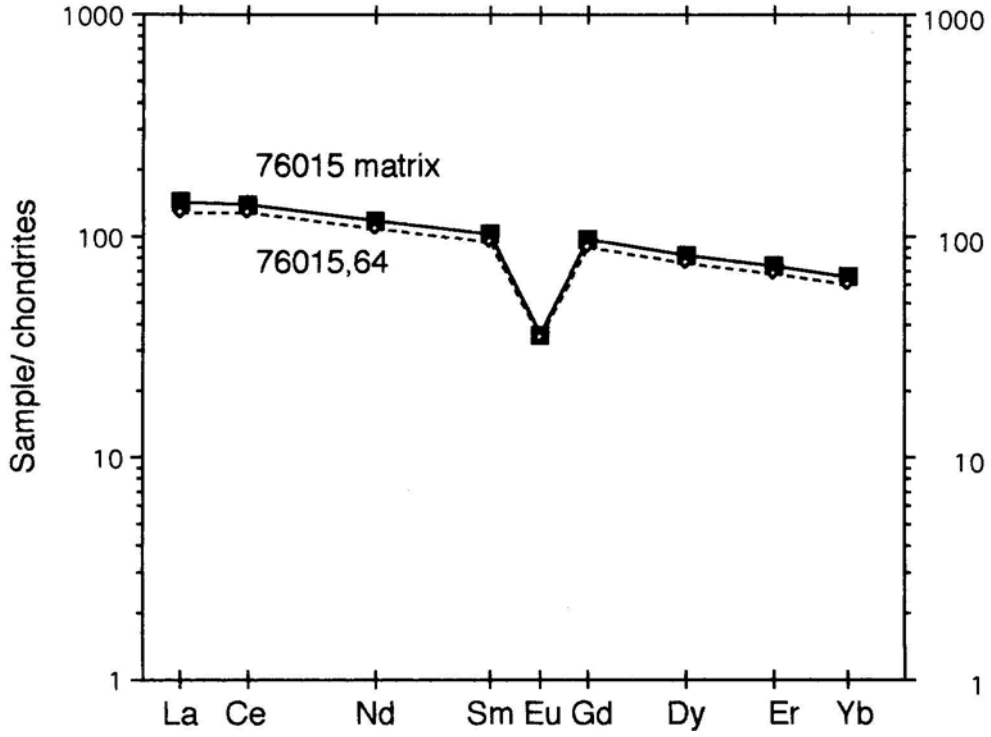

Figure 7: Normalized rare earth diagram for 76015. All subsamples have the same pattern and are similar to the matrix of 76215 and 76315. This sample provides a good reference for the other samples of the North Massif. Data from Hubbard et al. (1974).

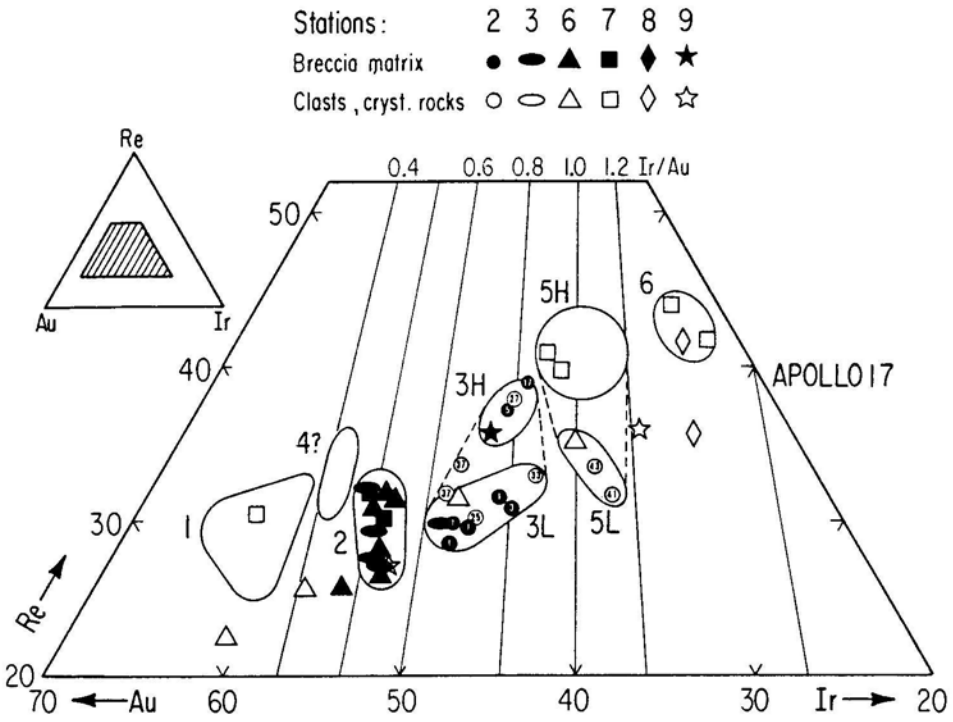

Figure 8: Ir-Au-Re compositions of Station 6 Boulder matrix all fall within Cluster 2 (see Higuchi and Morgan, 1975).

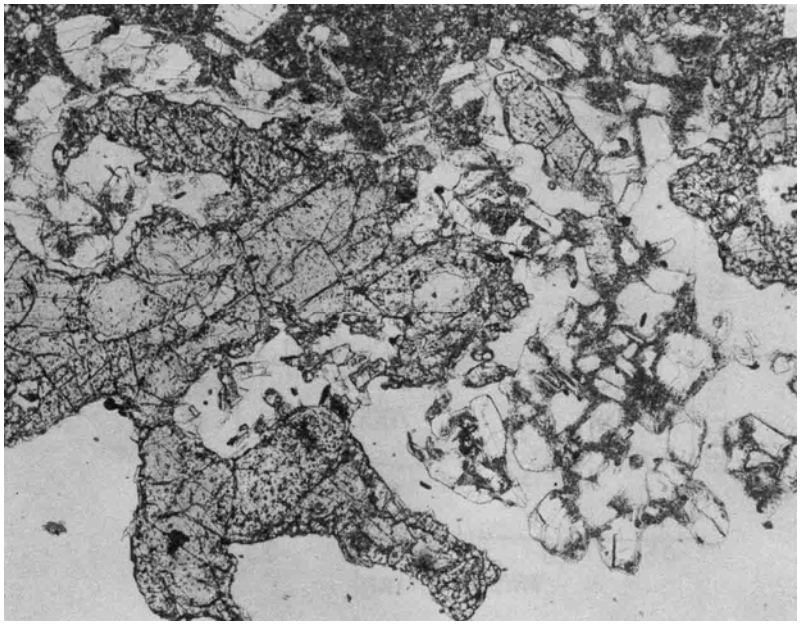

Figure 9: Large pyroxene grains and plagioclase laths in vesicular basalt clast (see Phinney, 1981). Scale is 4 x 5 mm.

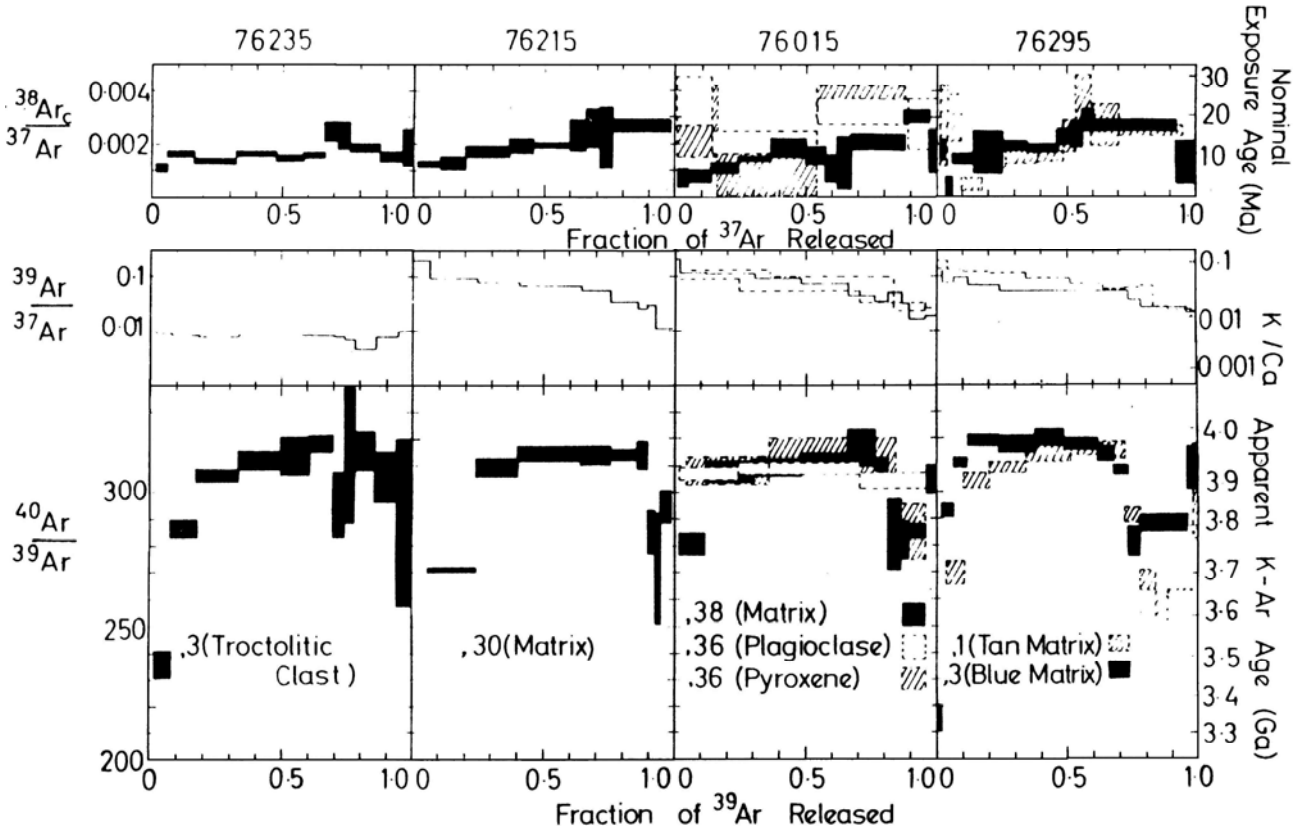

Figure 10: Apparent age and K/Ca as a function of Ar release by the Ar plateau technique for several matrix and mineral fractions of Station 6 Boulder samples. From Cadogan and Turner (1976).

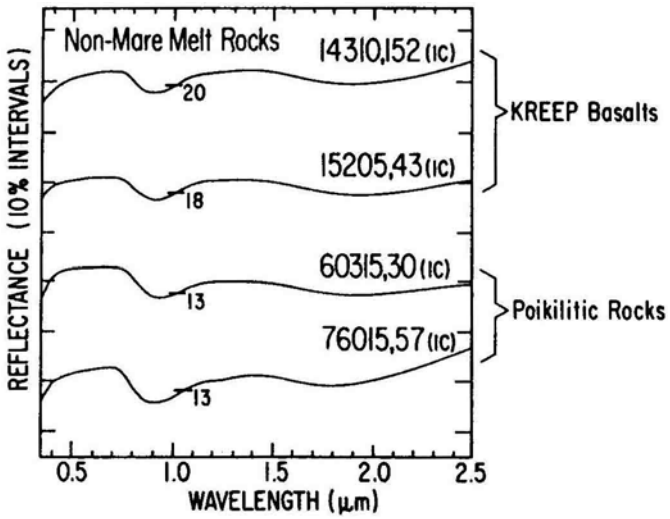

Figure 11: Comparison of reflectance spectra of poikilitic rocks (including 76015) and KREEP basalts. From Charette and Adams (1977).

MAGNETIC STUDIES

Pearce et al. (1974) and Gose et al. (1978) have carefully studied the remanent magnetization of 26 sub-samples from the Station 6 Boulder. The direction of magnetization of clast-free samples from unit B (including 76015) cluster fairly well after alternating field demagnetization. Gose et al. propose that the natural remanent magnetization of impact melt breccias is the vector sum of two magnetizations, a pre - impact magnetization and a partial thermoremanence acquired during breccia lithification.

SURFACE STUDIES

The thickness of the patina that developed on the T1 surface of 76015 (Fig. 3) is unusual and is a function of the exposure geometry of a partially to completely shielded cavity on top of the boulder. The Tl surface subtended a small solid angle and intercepted few large particles capable of eroding the surface, as is the case on the fully exposed exterior surface where there is a less well-developed patina due to constant steady-state erosion. There is a marked gradation in patina from the thick deposit of the partially shielded lip of the rock to a lack of patina in the completely shielded region. The thick deposit is made of accumulated glass splashes, pancakes, and presumably condensed vapor that may have come from the opposite face of the cavity.

The surface patina on 76015 has been carefully described by Blanford et al. (1975). The partially shielded part of the surface of 76015 has accumulated accretionary particles over a long period of time (22 m.y.?), while the exposed surface of 76015 reached a steady state of micrometeorite erosion and accumulated glass splashes. Accretionary particles are small objects adhering to the host surfaces. They include glass splashes, stingers, and pancakes as well as angular dust particles. Glassy accretionary particles are formed by fusion of target material by hypervelocity micrometeorites. Patina is the result of the accumulation of this fused material on nearby surfaces. High resolution examination of the stratigraphically oldest glass particles on the exterior surface of 76015 suggests that their surfaces have been altered by solar wind sputtering. Older particles have a granular appearance in contrast to the perfectly smooth appearance of the superposed younger particles.

Charette and Adams (1977) have determined the reflectance spectra of the surface of 76015 and report that the spectra of poikilitic rocks are similar to KREEP with a slight upturn at the high wavelength (Fig. 11). It would be interesting to determine the difference in spectra for patina-covered surfaces as compared to fresh surfaces (76015 is the ideal sample for such study).

EXPERIMENTAL

Experimental studies by Delano (1977) showed that 76015 has olivine as its liquidus phase at 0 kbars. Olivine + spinel coexist on

the liquidus in the pressure interval from 5 to 12 kbar. Olivine + spinel + orthopyroxene are simultaneously on the liquidus at 12 kbar. Orthopyroxene + spine] are the liquidus phases at pressures greater than 12 kbar (Fig. 12). Experimental phase relations of these experiments suggest that the 76015 composition does not represent magma derived by partial melting of either cosmic or differentiated source regions at any pressure on the Moon.

VUGS

This sample has numerous vugs and cavities with well-known orientation (Fig. 13). Morrison and Zinner (1975) used two of these cavities to study the possible directional variations in the flux of micro-meteorites and solar flare particles. Studies by Blanford et al. (1975) (Fig. 14) and Morrison and Zinner (1975) found no anisotropy in the flux of micrometeorites between the north direction and the ecliptic, whereas Hutcheon (using different samples) determined that the ecliptic flux was seven times as high as the flux from the south (see discussion in Zinner and Morrison, 1976).

Morrison and Zinner determined that there are 900 0.1 um craters produced per cm^2 per year per 2 n steradian. Based on their observation of numerous fresh 0.1 µm craters, they concluded that there is not more than an estimated maximum solar-wind erosion rate of 0.07 A/yr.

Morrison and Clanton (1979) have documented differences in the micro-meteorite populations and surface characteristics between the surface of 76015 that was exposed in the plane of the ecliptic and the surface that was exposed perpendicular to the ecliptic.

Carter et al. (1975) have studied the euhedral crystals of pyroxene, plagioclase, ilmenite, metallic iron, and troilite that line the vugs of 76015.

Phinney (1981) reports that large apatite crystals occur in the vugs of 76015 as honey-yellow, transparent, single crystals up to 1 mm in greatest dimension. They are found to be doubly terminated and loosely adhering to the cavity walls. Large beta-cristobalite crystals and wiry and dendritic metallic Cu are also reported in these cavities.

PROCESSING

A slab and a column were cut from the center of this rock (see maps in Phinney, 1981). A second slab and column were cut at right angles to the first slab in 1988. A large piece (330 g) has been used for public display.

The largest piece remaining (,18) weighs 1307 g and is stored at Brooks Air Force Base. The second largest piece (,19) weighs 630 g. There are 30 thin sections.

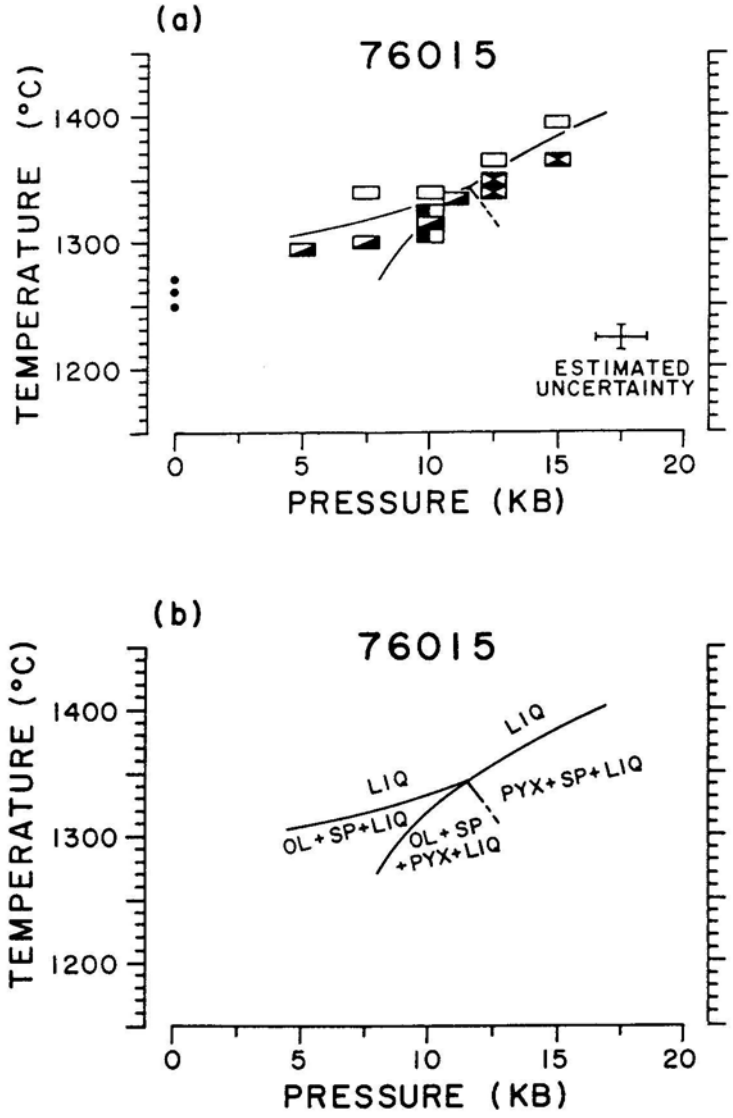

Figure 12: Melting relations of 76015 as a function of temperature and pressure. From Delano (1977).

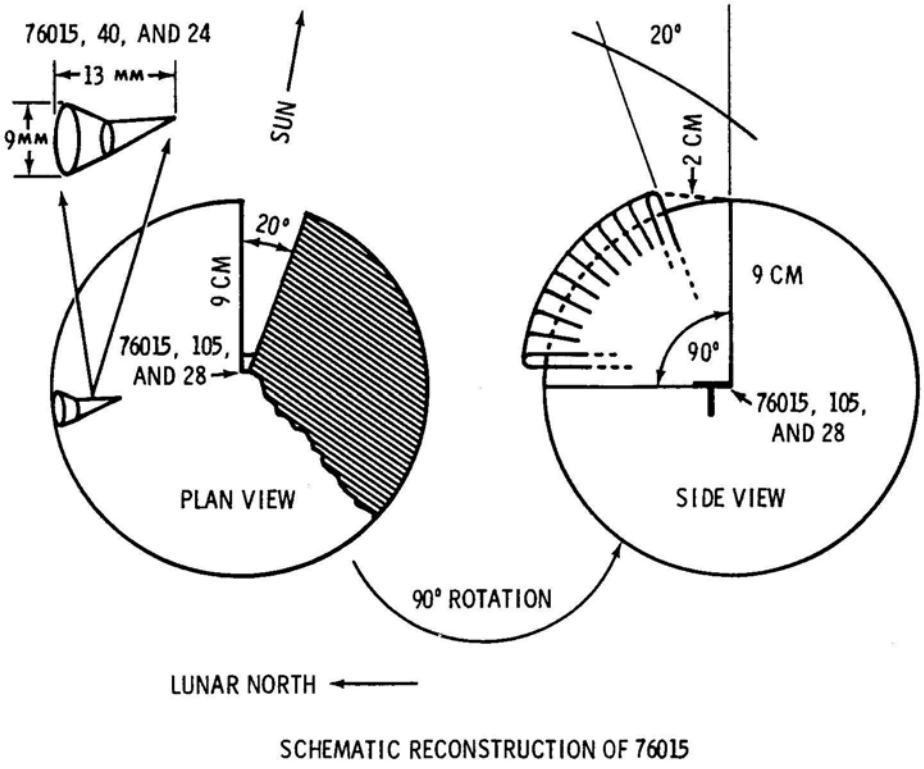

Figure 13: Orientation and exposure geometry of 76015,105,24 and,40. From Morrison and Zinner (1975).

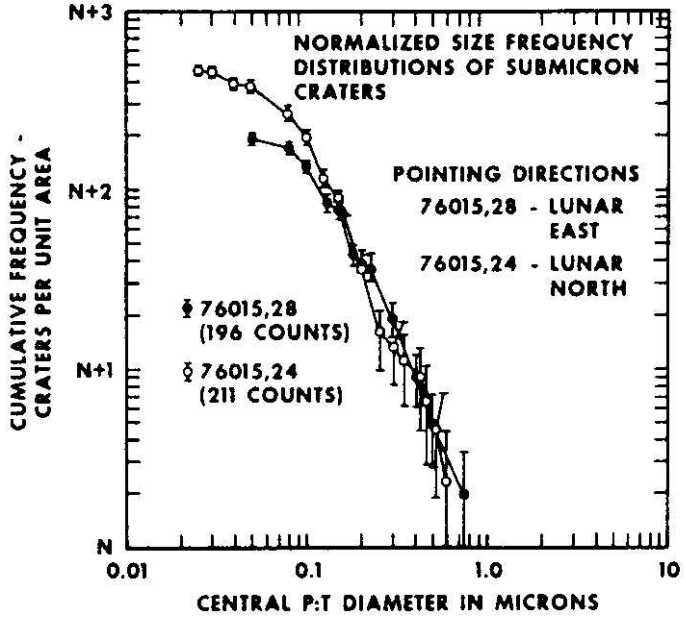

Figure 14: Size frequency distributions of zap pits on oriented surfaces of 76015. From Blanford et al. (1975).

Table 1: Whole-rock chemistry of 76015.
a) Rhodes et al. (1974a); Hubbard et al. (1974); b) Palme et al. (1978)
See also Wiesmann and Hubbard (1975) and Phinney (1981).

Split Technique	,22M (a) XRF, IDMS	,37M (a) XRF, IDMS	,41M (a) XRF, IDMS	,64M (a) XRF, IDMS	,12 (b) XRF, INAA
SiO_2 (wt%)	46.16	46.38	46.38	46.59	46.52
TiO_2	1.52	1.55	1.53	1.48	1.54
Al_2O_3	17.17	17.78	17.77	18.00	17.86
Cr_2O_3	–	–	–	–	0.19
FeO	9.81	9.65	9.07	9.10	8.08
MnO	0.13	0.13	0.12	0.12	0.11
MgO	13.03	12.40	12.67	12.43	12.57
CaO	10.77	11.13	11.11	11.10	10.99
Na_2O	0.70	0.72	0.69	0.75	0.68
K_2O	0.26	0.26	0.26	0.29	0.24
P_2O_5	0.27	0.29	0.29	0.28	0.28
S	0.09	0.06	0.08	0.08	0.39
Nb (ppm)					32
Zr	490	515	507	484	480
Hf	12.5	12.7	–	–	11.81
Ta					1.62
U	1.46	1.59	1.96	1.48	1.2
Th	5.44	5.64	5.56	5.41	4.18
Y					112
Sr	172	178	177	174	180
Rb	6.41	6.67	6.57	7.46	–
Li	18.3	19.8	21.6	18.5	17.7
Ba	348	362	358	354	340
Cs					0.20
Ni					1140
Co					90.2
Sc					16.7
La	–	34.3	33.4	29.9	33.8
Ce	83.3	85.9	84.9	78.4	89.2
Nd	52.8	54.4	54.0	49.3	54
Sm	14.9	15.3	15.2	14.0	14.11
Eu	1.94	2.02	1.99	1.97	1.99
Gd	18.7	19.0	18.9	17.6	18.1
Tb					3.04
Dy	19.5	20.0	19.9	18.3	19.9
Er	11.5	11.8	11.7	10.9	–

Table 1: (Concluded).

Split Technique	,22M (a) XRF, IDMS	,37M (a) XRF, IDMS	,41M (a) XRF, IDMS	,64M (a) XRF, IDMS	,12 (b) XRF, INAA
Yb	10.6	11.0	10.8	10.0	11.43
Lu	–	–	1.30	1.50	1.55
Ga					–
F					45.8
Cl					6.9
Ge (ppb)					–
Ir					43
Au					18

Table 2: Trace element data for 76015. Concentrations in ppb.
From Higuchi and Morgan (1975).

	Sample 76015,77 matrix
Ir	3.41
Os	
Re	0.315
Au	1.89
Pd	
Ni (ppm)	135
Sb	1.02
Ge	164
Se	76
Te	2.7
Ag	1.02
Br	46.8
In	
Bi	0.22
Zn (ppm)	2.8
Cd	3.2
Tl	0.67
Rb (ppm)	5.77
Cs	266
U	1490

Table 3: Rb-Sr composition of 76015.
Data from Nyquist et al. (1974).

Sample	76015,22M	,37M	,41M	,64M
wt (mg)	52.3	53.5	63.6	51.5
Rb (ppm)	6.41	6.67	6.57	7.46
Sr (ppm)	171.8	177.5	176.6	173.8
$^{87}Rb/^{86}Sr$	0.1079 ± 9	0.1088 ± 9	0.1076 ± 9	0.1242 ± 10
$^{87}Sr/^{86}Sr$	0.70589 ± 5	0.70605 ± 5	0.70589 ± 11	0.70693 ± 6
T_B	4.39 ± 0.07	4.45 ± 0.07	4.40 ± 0.11	4.40 ± 0.07
T_L	4.45 ± 0.07	4.52 ± 0.07	4.45 ± 0.11	4.44 ± 0.07

B = Model age assuming I = 0.69910 (BABI + JSC bias)
L = Model age assuming I = 0.69903 (Apollo 16 anorthosites for T = 4.6 b.y.)